
THE IMPACT OF DEEP LEARNING AID ON THE WORKLOAD AND INTERPRETATION ACCURACY OF RADIOLOGISTS ON CHEST COMPUTED TOMOGRAPHY: A CROSS-OVER READER STUDY.

Anvar Kurmukov¹, Valeria Chernina¹, Regina Gareeva¹, Maria Dugova¹, Ekaterina Petrash¹, Olga Aleshina¹, Maxim PISOV¹, Boris Shirokikh¹, Valentin Samokhin¹, Vladislav Proskurov¹, Stanislav Shimovolos¹, Maria Basova¹, Mikhail Goncahrov¹, Eugenia Soboleva¹, Maria Donskova¹, Farukh Yaushev¹, Alexey Shevtsov¹, Alexey Zakharov¹, Talgat Saparov¹, Victor Gombolevskiy¹, and Mikhail Belyaev¹

¹AUMI.AI

June 13, 2024

ABSTRACT

Interpretation of chest computed tomography (CT) is time-consuming. Previous studies have measured the time-saving effect of using a deep-learning-based aid (DLA) for CT interpretation. We evaluated the joint impact of a multi-pathology DLA on the time and accuracy of radiologists' reading. 40 radiologists were randomly split into three experimental arms: control (10 radiologists), unaware of DLA capabilities who interpret studies without assistance; informed group (10 radiologists), who underwent a briefing about which pathologies DLA detects, but performed readings without DLA; and the experimental group (20 radiologists), who interpreted half studies with DLA, and half without. Every arm used the same 200 CT studies retrospectively collected from BIMCV-COVID19 dataset; each radiologist provided readings for 20 CT studies. We compared participants' interpretation time, and accuracy of their diagnostic report in terms of sensitivity and specificity with respect to 12 pathological findings.

Mean reading time per study was 15.6 minutes [SD 8.5] in the control arm, 13.2 minutes [SD 8.7] in the informed arm, 14.4 [SD 10.3] in the experimental arm without DLA, and 11.4 minutes [SD 7.8] in the experimental arm with DLA. Mean sensitivity and specificity were 41.5 [SD 30.4], 86.8 [SD 28.3] in the control arm; 53.5 [SD 22.7], 92.3 [SD 9.4] in the informed non-assisted arm; 63.2 [SD 16.4], 92.3 [SD 8.2] in the experimental arm without DLA; and 91.6 [SD 7.2], 89.9 [SD 6.0] in the experimental arm with DLA. DLA speed up interpretation time per study by 2.9 minutes ($CI_{95}[1.7, 4.3]$, $p < 0.0005$), increased sensitivity by 28.4 ($CI_{95}[23.4, 33.4]$, $p < 0.0005$), and decreased specificity by 2.4 ($CI_{95}[0.6, 4.3]$, $p = 0.13$).

Of 20 radiologists in the experimental arm, 16 have improved reading time and sensitivity, two improved their time with a marginal drop in sensitivity, and two participants improved sensitivity with increased time. Overall, DLA introduction decreased reading time by 20.6%.

1 Introduction

According to the Royal College of Radiology's Workforce Census reportThe Royal College of Radiologists [2024], the UK National Healthcare System faces a 29% shortfall in clinical radiologists, projected to increase to 40% by 2027. Simultaneously, the Association of American Medical CollegesAssociation of American Medical Colleges [2021] anticipates a shortage between 10300 and 35600 of "Other specialities", including radiologists, by 2034 in the US. The Radiological Society of North America also reportsRadiological Society of North America [2022] a global shortage of radiologists. Concurrently, the amount of performed Computed Tomography studies rises, with a 7% annual increase in the UK; a similar trend is observed in the US, where it nearly doubled from 2010 to 2020Richards et al. [2022],

Winder et al. [2021]. This combination of a dwindling workforce and escalating workload underscores an urgent need for enhanced efficiency.

Recent studies have showcased the potential of modern deep learning in detecting and delineating a variety of pathologies on computed tomography, magnetic resonance imaging and x-ray studies Ueda et al. [2023], Rao et al. [2021], Çallı et al. [2021], Shirokikh et al. [2022]. While these systems match human performance metric-wise, their real-world clinical impact remains under-investigated Liu et al. [2019], Gorenstein et al. [2023]. A recent review by Liu et al., highlights that although deep learning algorithms often perform comparably to healthcare professionals, few studies compare their performance on external datasets, with direct comparison with humans Liu et al. [2019].

Moreover, while many studies assess the accuracy of deep-learning-based systems with application to medical imaging diagnostics, only a few authors compare the efficiency of radiologists, with and without the deep-learning-based aid (DLA) in terms of working time. Existing results suggest a 10-31% time decrease for chest radiography, 30% time decrease for hand radiographs. Bennani et al. [2023], Ahn et al. [2022], Eng et al. [2021]

Research of DLA influence on workload with respect to CT is limited. One study analysed the effect of multi-task DLA on chest CT interpretation times Yacoub et al. [2022]. The average effect for three participant radiologists was reported to be 22.1% time reduction. However, this study did not assess the impact on examination accuracy, and time recordings were performed manually by the participants. Another study Abadia et al. [2022] assessed a non-inferiority of AI system compared to radiology reports with 8.4% increase in sensitivity with respect to lung nodule detection of patients with complex lung diseases. In addition, the authors demonstrated a 78% reduced CT evaluation time (from 2:44 minutes to 35.7 seconds on average). However, the latter result was demonstrated on 20 random cases (out of 143), all of which were positive for lung cancer, based on times recorded from a single radiologist after a one-month washout.

In present work, we tested how a multi-pathology deep-learning-based aid affects radiologists' workload and accuracy. Our study design allows for paired comparisons on the image level (the same CT study was annotated with and without DLA) and on the radiologist level (the same radiologists assessed studies with and without DLA). We demonstrated the overall positive effect of DLA examination on both workload (reduced time) and detection accuracy (increased sensitivity, with preserved level of specificity).

2 Methods

We evaluated a deep-learning-based software designed to assist in diagnosing 12 chest and abdomen pathologies on CT scans, including lung nodules, features of viral pneumonia, emphysema and pleural effusion, lymphadenopathy in the intrathoracic lymph nodes, aorta and pulmonary trunk enlargement, coronary calcium, adrenal lesions, ribs and vertebrae fractures, and vertebrae mineral density. We performed paired comparisons in two distinct ways: first, by enabling the same radiologists to evaluate different CT studies with and without DLA assistance, and second, by allowing various radiologists to assess the same CT studies, both with and without the DLA. We measured the joint effect on workload and performance and analysed inter-/intra-readers and inter-group variability.

2.1 Software

EfficientReadCT (version 1.0.0, AUMI.AI) was used for the purposes of this study. It is a commercially available deep-learning-based computer aid diagnosis system developed for detection of various pathologies on CT studies. It automates morphological measurements and provides diagnostic suggestions for 12 pathologies in a structured form according to the international guidelines MacMahon et al. [2017], Francone et al. [2020], Occhipinti et al. [2019], Karkhanis and Joshi [2012], Munden et al. [2018], European Society of Cardiology, Glazer and Mayo-Smith [2020], He et al. [2019], Genant et al. [1993], International Society for Clinical Densitometry [2023], see Supplementary materials Table 2.

2.2 Study design

The primary aim of this study was to estimate the effect of DLA interpretation on CT reading times. The secondary goal was to estimate the effect on examination accuracy. Radiologists were not informed that their reading time was being recorded. They were informed that the diagnostic accuracy of their readings would be measured. They were paid regardless of their performance.

Radiologists assessed the studies from their personal computers using the RadiAnt DICOM viewer (v.2023.1). Each study was accompanied by patient age, sex and anamnesis and diagnostics task e.g. "49 y.o. woman with cough and expectoration". For each study, the participants were asked to fill up a web form pre-filled either with a standard report describing the organs and systems included in the scan, without pathological findings, or report with DLA results,

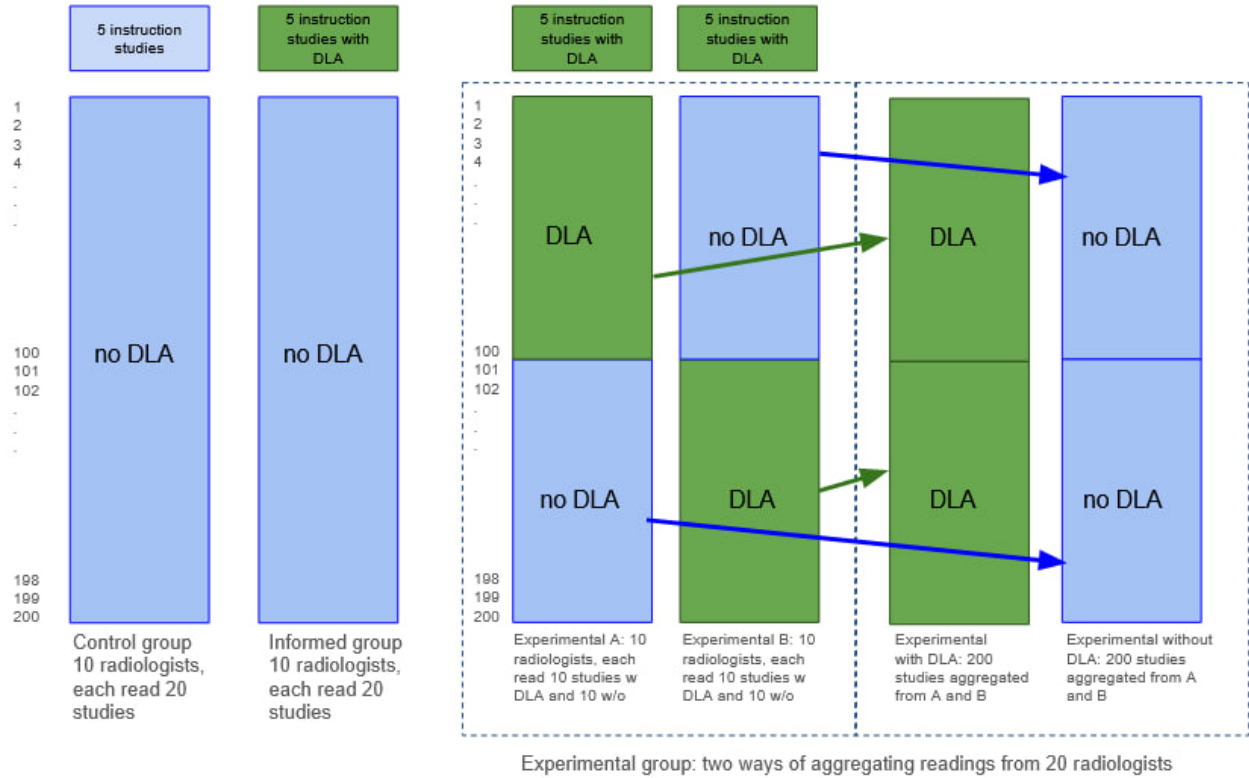


Figure 1: Study design.

see examples in Supplementary Table 1. After interpreting a study, the participant submitted the report and was not able to edit it later. Time spent on the interpretation of a single study was automatically recorded as the time between pressing the “Start new study” and “Submit a report” buttons in the webform. Participants were asked not to take breaks during the interpretation of a single study but could make any number of breaks between the studies. Participants were instructed to finish all their studies in a single working day.

We enrolled 40 radiologists and divided them into three groups, consisting of 10, 10 and 20 radiologists, see Figure 1 and group descriptions below. Each participant annotated 20 unique CT studies. In total, we used 200 unique CT studies for the experiment; each study was annotated independently by four radiologists.

CT studies were selected from publicly available data collection approved for research purposes.²⁷ Studies interpretation was performed retrospectively without affecting patient treatment plans.

2.2.1 Groups without DLA

The first 10 radiologists, mean working experience 9.8 years [SD 2.8], were a control group who annotated the experimental data without DLA. The purpose of this group was three-fold. First, to estimate the baseline reading time and accuracy. Second, to compare the performance of the participants with the accuracy of the original radiological reports. This established the effect of non-clinical/non-prospective experimental design. Third, to compare with radiologists in the informed group.

The second group of 10 radiologists, mean working experience 8.3 years [SD 3.1], i.e. “informed group” also annotated experimental data without the DLA. However, before the experiment, they received five CT studies processed by the DLA which covered all pathologies known to it. The purpose of these five studies was to familiarise participants with the DLA capabilities which include pathologies rarely mentioned in the readings during routine examination, such as loss of vertebrae mineral density, adrenal incidentalomas, and others. We hypothesised that radiologists who are aware that the DLA detects such pathologies would also pay more attention to them, even without the DLA.

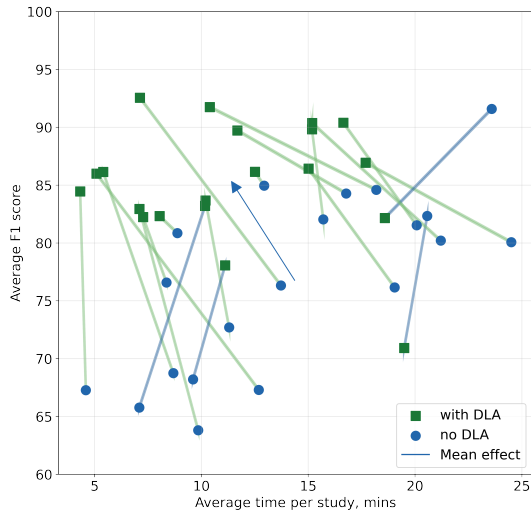


Figure 2: Time vs F1 score in experimental group by participants. Each line represents one participant from the experimental arm.

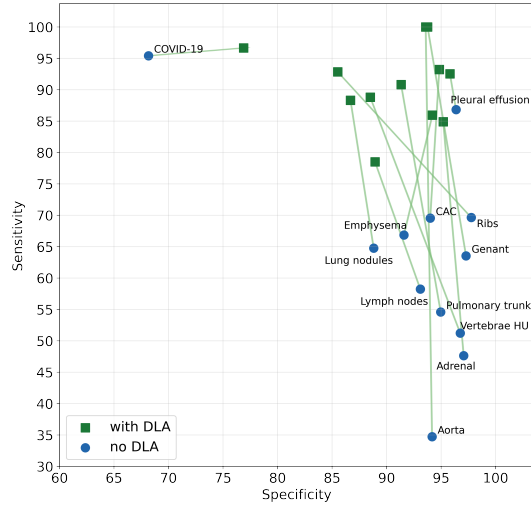


Figure 3: Sensitivity and specificity by pathologies between participants with DLA and without in the experimental arm.

2.2.2 The experimental group

The experimental group consisted of 20 radiologists, mean working experience 9.3 years [SD 3.4], each interpreted studies with and without the DLA. Before the experiment, all participants from this group received five CT studies with deep learning-generated overlay. During the experiment, each participant annotated half of their studies with the DLA, and half - without. Studies with and without the DLA were read in random order to mitigate the potential effect of fatigue to the end of the experiment session Taylor-Phillips and Stinton [2019]. Studies were distributed in such a way, that each of 200 studies were once annotated with the DLA, and once - without.

The experimental group could be seen in two ways, see Figure 1. First, as two independent groups: experimental A and experimental B each consists of 10 participants. Each radiologist in either group interpreted 20 unique studies (10 with the DLA and 10 without). For each radiologist this allowed us to compare the performance and reading time on 10 studies without the DLA versus 10 studies with DLA (a crossover design).

Second, if a study was analysed with the DLA in group A, it was analysed without the DLA in group B. Thus, the experimental group could be seen as 200 studies analysed once without the DLA (by 20 radiologists, each provided 10 readings) and once with the DLA (by the same 20 radiologists, each provided 10 readings). We used these two groups to derive the effects of the DLA introduction.

2.3 Validation data

We used CT studies from the BIMCV COVID-19+ collection Vayá et al. [2020]. We selected 205 CT studies without contrast enhancement with chest region (Th1 to Th12 vertebrae present). Of 205 subjects, five studies were used to familiarise participants with the experiment interfaces, and the DLA capabilities in case of informed and experimental groups. The remaining 200 studies were used for the experiment, of which 97 (48.5%) were male, mean age 67.7 years [SD 14.5], and 103 (51.5%) were female, mean age 62.7 [SD 16.9]. We manually extracted BIMCV annotations from medical reports associated with the CT studies, see details in the Supplementary materials “Text annotation”.

2.3.1 Ground truth development

To obtain the ground truth labels, we compared six sources of labels: extracted from the original medical reports, from radiologists from each experimental arm, and generated by the DLA system. If all six sources agreed on a specific diagnosis, we accepted it as the ground truth. Otherwise, if any of the six sources disagreed, the study was reviewed by an experienced radiologist for this particular pathology without DLA.

The annotation of severity of pathologies (e.g. aorta enlargement > 50 mm, Agatston’s score > 300) was performed in a second round of annotation with access to DLA. Pleural effusion was excluded from the severity analysis, because it often requires the analysis of drained fluids, which was not possible in the retrospective setup.

Table 1: International guidelines on selected pathologies diagnostics. Criteria for lymphadenopathy, aorta enlargement, vertebrae fractures and COVID-19 were simplified.

Pathology	Location	low	moderate	severe
lung nodules MacMahon et al. [2017]	Chest	<6 mm (100 mm ³)	6-8 mm (100-250 mm ³)	>8 mm (>250 mm ³)
COVID-19 Francone et al. [2020]	Chest	1-25% lobar involvement	25-50% lobar involvement	>50% lobar involvement
emphysema Occhipinti et al. [2019]	Chest	isolated bullas < 10mm, LAA _{-950insp} 1-5%	LAA _{-950insp} 6-14%	LAA _{-950insp} ≥ 14%
lymphadenopathy Munden et al. [2018]	Chest	short axis < 10mm	short axis 11-15 mm	short axis >15 mm
ascending aorta European Society of Cardiology	Chest	-	diameter 40-49 mm	diameter >50 mm
descending aorta European Society of Cardiology	Chest	-	diameter 31-39 mm	diameter >40 mm
descending aorta European Society of Cardiology	Abdomen	-	diameter 26-30 mm	short axis >30 mm
pulmonary artery Munden et al. [2018]	Chest	diameter 29-30 mm	diameter 31-33 mm	diameter 31-33 mm
coronary calcium Munden et al. [2018]	Chest	Agatston score 1-100	Agatston score 101-300	Agatston score >300
adrenal lesions Glazer and Mayo-Smith [2020]	Abdomen	short axis < 10mm, density <10HU	short axis 11-39mm, density >10HU	short axis >40mm, density >10HU
ribs fractures He et al. [2019]	Bones	consolidated fracture	nondisplaced fracture	displaced fracture
vertebral fractures Genant et al. [1993]	Bones	height reduction 20-25%	height reduction 26-40%	height reduction >40%
vertebral density International Society for Clinical Densitometry [2023]	Bones	100-150 HU	<100 HU	-

Dataset statistics on the number of pathologies with different severity are available in the Supplementary materials Tables 3-4.

2.4 Statistical analysis

Statistical analysis were performed in Python, Wilcoxon signed-rank test was used for paired comparisons. Two-sided 95% confidence intervals were assessed via bootstrapping (over studies) with 1000 repetitions. We set the alpha significance level at 0.03.

3 Results

3.1 BIMCV vs Control vs Informed

First, we compare the control group with the results derived from the original medical reports. For most of the analysed pathologies we observe no statistically significant differences in sensitivity and specificity, except for emphysema, coronary calcium and lymph nodes, for which radiologists in the control group demonstrate higher sensitivity; lung nodules, for which original reports have higher sensitivity; and infiltration and consolidation of lung tissue during COVID and lung’s nodules, for which original reports have higher specificity. Averaged over 12 pathologies, sensitivity is higher in the control group by 10.2 points (CI [5.5, 14.3], $p = 0.026$), there is no statistically significant difference in specificity (CI [0.1, 2.6], $p = 0.23$), see Table 1. Tables with pathology-wise classification metrics for all arms are provided in the Supplementary materials Table 5.

Second, we compare the control and informed groups. On average sensitivity is higher in the informed group by 11.9 points (CI [7.1, 17.1], $p = 0.016$), the differences in specificity are not statistically significant (CI [2.0, 5.4], $p = 0.16$). This result supports our initial hypothesis that familiarity with DLA pathologies increases participants’ awareness of them.

Finally, we report that reading times were 2.4 fewer minutes (CI [0.8, 4.0], $p = 0.0007$) in the informed group (on average per study). We attribute this result to individual differences among radiologists in interpretation time, rather than to the familiarity with DLA, see next section.

3.2 Experimental group

3.2.1 Inter-reader variability

First, we compare the Experimental groups A and B in terms of time and performance to measure inter-radiologists’ differences, while preserving the reading conditions, see Table 1. Both groups analysed the same 200 CT studies, half

with DLA and half without. There were no statistically significant differences between the groups in terms of sensitivity (CI $[-9.5, 4.1]$, $p = 0.57$), and specificity (CI $[-0.7, 2.8]$, $p = 0.34$). However, participants in Experimental group A spent on average 4.06 more minutes (CI $[2.6, 5.4]$, $p < 0.0001$) on reading a single study. These results demonstrate that there is low inter-group variability in performance but high variability in time, meaning that the effect on workload could only be measured in a cross-over fashion, i.e., comparing reading time of radiologists with themselves with and without DLA.

Table 2: Time and performance metrics of radiologists in different experimental groups. Mean (std) are averaged over 12 pathologies. Time mean (std) averaged over studies.

Group/Metrics	Sensitivity	Precision	Specificity	F1	Time, mins
BIMCV annotation	31.3 (30.7)	77.8 (20.0)	96.5 (5.5)	37.4 (27.5)	n/a
Control	41.5 (30.5)	76.0 (22.6)	95.2 (7.3)	51.7 (25.5)	15.6 (8.5)
Informed	53.5 (22.7)	73.2 (16.3)	91.5 (9.4)	57.8 (16.8)	13.2 (8.7)
Experimental A	76.1 (11.5)	77.0 (15.4)	91.6 (7.8)	75.5 (10.7)	10.9 (7.5)
Experimental B	78.7 (9.9)	75.8 (12.2)	90.6 (5.9)	76.3 (7.3)	14.9 (10.4)
Experimental without DLA	63.2 (16.4)	77.1 (13.7)	92.3 (8.2)	67.8 (11.1)	14.4 (10.3)
Experimental with DLA	91.6 (7.2)	76.4 (14.3)	89.9 (6.1)	82.5 (9.5)	11.4 (7.8)
Automated (no radiologist)	89.9 (8.3)	73.0 (14.4)	87.3 (9.2)	79.5 (9.1)	n/a

3.2.2 Time and performance

Figure 2 demonstrates the joint effect on performance and workload from DLA introduction. 16 out of 20 participants benefited in terms of both time and F1 score, two participants substantially increased their F1 score, with increased workload, two participants examined studies faster with DLA, but with lower average F1 score. Overall, while using DLA participants had higher sensitivity by 28.4 points (CI $[23.5, 33.5]$, $p = 0.0005$), differences in specificity were not statistically significant (CI $[0.7, 4.3]$, $p = 0.13$), and F1 score is higher by 14.8 points (CI $[10.7, 18.7]$, $p = 0.0010$).

The average time saved per study was 2.9 minutes (CI $[1.7, 4.3]$, $p = 0.0005$) per study, or 20.6% (CI $[14.9\%, 37.7\%]$). On an individual radiologists level, DLA introduction decreased reading time for 18 out of 20 participants, see Figure 2. For each of 18 radiologists, the decrease in examination time was statistically significant with $p < 0.0001$. Figure 3 demonstrates the effect on individual pathologies, the increase in sensitivity is especially apparent for pathologies determined by morphological measurements, such as the diameter of the aorta or pulmonary artery, vertebrae fractures and density. In Supplementary materials we provide radiologists-wise metrics for all groups, Table 6.

3.2.3 Findings severity

To analyse how radiologists' accuracy changes depending on the severity of pathologies, we computed stratified sensitivity, see Table 3. We do not report Specificity as True Negatives could not be classified for severity. We also do not report Precision, because when a radiologist describes a finding which is not present (a False Positive), it is too arbitrary to decide, which severity level was implied from the text description.

Table 3: Sensitivity stratified by the findings' severity. Mean (std) are averaged over 12 pathologies.

	low	moderate	severe
BIMCV annotation	24.8 (33.4)	35.4 (37.2)	47.2 (35.1)
Control	39.2 (30.9)	48.1 (41.4)	60.6 (25.1)
Informed	40.3 (28.1)	64.0 (30.8)	67.9 (27.9)
Experimental A	65.4 (21.1)	81.2 (17.3)	89.1 (12.1)
Experimental B	64.8 (23.0)	81.5 (16.3)	85.7 (10.6)
Experimental without DLA	48.0 (29.5)	69.2 (20.2)	81.0 (16.1)
Experimental with DLA	82.2 (15.8)	93.5 (11.8)	93.8 (7.3)
Automated (no radiologist)	70.7 (29.8)	93.8 (8.4)	93.3 (12.3)

As expected, the sensitivity of radiologists increases when dealing with conditions of higher severity, in every arm. For findings of low severity, we observe an increase in sensitivity from 39.4 (CI $[0.0, 98.3]$) in the control group, to 48.1 (CI $[0.0, 96.6]$) in the experimental group without DLA, and to 82.3 (CI $[28.6, 100.0]$) in the experimental group

with DLA. For moderate severity findings we observe an increase in sensitivity from 44.5 (CI [0.0, 100.0]), to 66.3 (CI [26.7, 100.0]) and 94.0 (CI [57.1, 100.0]) in the control group, experimental group without DLA and with DLA respectively.

Finally, for findings of high severity, sensitivity increased from 60.6 (CI [10.3, 100.0]) in the control group, to 80.9 (CI [40.0, 100.0]) in the experimental group without DLA and 93.8 (CI [66.7, 100.0]) in the experimental group with DLA.

Wide confidence intervals are due to the relatively low number of positive findings for each severity, see Supplementary materials for severity statistics in Table 3.

4 Discussion

Numerous studies have explored the accuracy of AI algorithms applied to radiography; however, only a handful have compared the efficiency of radiologists, with and without DLA assistance, in terms of working time. Eng et al. reported a 30% decrease in workload time for skeletal age assessment from hand radiographs, alongside a 9.5% increase in accuracy Eng et al. [2021]. A similar estimate of 31% saved time was reported by Bennani and colleagues, who enlisted 12 radiologists with varying work experience to analyse five lung pathologies on chest X-rays Bennani et al. [2023]. Conversely, Ahn et al. reported a smaller effect of a 10% decrease in workload from AI for similar tasks, albeit with a significant increase in sensitivity Ahn et al. [2022]. These studies underscore the potential of AI to enhance both efficiency and accuracy in radiography.

The impact of deep learning aid assistance on workload for CT readings remains underexplored. Abadia et al. demonstrated the non-inferiority of an AI system compared to radiology reports for detecting lung cancer in patients with complex lung diseases Abadia et al. [2022]. They also reported significantly reduced CT evaluation times. However, the latter result was demonstrated using a limited number of cases based on reading times of a single radiologist. Yacoub et al. explored the effects of a multi-pathology DLA system for thoracic and abdominal CT on radiologists' working time, reporting a 22% reduction in workload from three radiologists Yacoub et al. [2022]. Main limitation of this study is that the authors did not address the potential performance trade-off associated with reduced working time.

In this work, we demonstrated that DLA introduction reduces interpretation time per study by 2.9 minutes (20.8%), simultaneously increasing sensitivity by 28.4, and preserving the same level of specificity. Importantly, we showed that the effect of introducing DLA assistance, is of the same magnitude as the effect of changing the radiologist, which is 4.06 minutes (CI [2.6, 5.4]). This result underlines the importance of radiologists-wise cross-over study design. We also demonstrated that while all of selected pathologies benefited from DLA introduction in sensitivity, pathologies diagnosed based on morphological measurements benefited more.

Our study has several limitations. First, we used retrospective data. Second, findings derivation methodology focused on all pathologies present on image, this resulted in relatively low metrics of annotations extracted from original medical reports. The discordance in accuracy between findings extracted from medical reports and findings described from CT readings retrospectively is a known phenomena Gatt et al. [2003]. Some of the findings that we included in the analysis might not have been clinically relevant for the specific patient, such as trace amounts of pleural effusion, decrease in bone density or consolidated ribs fractures. Especially because we used retrospective data from the emergency department from the COVID-19 pandemic period. To estimate the magnitude of the non-clinical retrospective design we included a control group of 10 radiologists who interpreted the scans without any aid or knowledge about DLA capabilities, and found the effect to be about 10.2 points of sensitivity. Third, we did not perform a power analysis prior to study start. However, the number of participants and studies in our experiment matches or outnumbers similar works on CT and chest radiography Bennani et al. [2023], Ahn et al. [2022], Yacoub et al. [2022], Abadia et al. [2022]. Finally, an interesting direction for future work would be to investigate the collateral effect of DLA systems on the accuracy of radiologists' diagnoses of pathologies not included in the DLA scope. This could provide further insights into the potential and limitations of DLA systems in radiology.

4.1 Conclusion

Current development of computer vision deep-learning-based AI systems for pathology detection and morphology annotation is approaching the best of human experts and outperforms an "average" radiologist who works without computer aid assistance. Radiologists augmented with DLA systems spend less time on CT examination and are more accurate with regard to pathologies highlighted by DLA. Results from independent research groups suggest a similar estimate of a 20% workload reduction effect from multi-pathology DLA introduced into clinical practice.

In this study we demonstrated that the use of deep-learning-aid for CT interpretation decreases total time spent on CT interpretation and increases sensitivity for 12 pathologies included in the DLA scope: lung nodules, features of viral

pneumonia, emphysema and pleural effusion, lymphadenopathy, aorta and pulmonary trunk enlargement, coronary calcium, adrenal lesions, ribs and vertebrae fractures, and vertebrae mineral density. These results suggest that the integration of deep-learning-aid in radiology practice holds great promise for improving efficiency and diagnostic accuracy, ultimately benefiting patient care.

4.2 Contributors

Study design: Mikhail Beliaev, Valeria Chernina, Maria Dugova, Ekaterina Petrash, Anvar Kurmukov. Conceptualisation: Mikhail Beliaev, Regina Gareeva, Victor Gomboleviskiy. Data management: Maxim Pisov, Vladislav Proskurov, Anvar Kurmukov, Maria Basova, Maria Dugova, Ekaterina Petrash, Valeria Chernina, Olga Aleshina. Software development: Maxim Pisov, Boris Shirokikh, Valentin Samokhin, Stanislav Shimovolos, Mikhail Goncharov, Eugenia Soboleva, Maria Donskova, Farukh Yaushev, Alexey Shevtsov, Alexey Zakharov, Talgat Saparov. Statistical analysis: Anvar Kurmukov, Maria Basova. Writing: Anvar Kurmukov, Mikhail Beliaev, Victor Gomboleviskiy.

4.3 Data Sharing

Validation data are a subset of a public dataset BIMCV COVID-19+, models' training data and pretrained models' weights will not be made publicly available due to intellectual property-related constraints. Studies unique identifiers, records collected during the experiment (per-radiologist examination time, examination labels, ground truth annotations), are publicly available at <https://zenodo.org/doi/10.5281/zenodo.10965415>.

References

- The Royal College of Radiologists. Clinical radiology census reports, 2024. URL https://www.rcr.ac.uk/media/qs0jnfmv/rcr-census-clinical-radiology-workforce-census_2022.pdf.
- Association of American Medical Colleges. The complexities of physician supply and demand: Projections from 2019 to 2034, June 2021. URL <https://www.aamc.org/media/54681/download?attachment>.
- Radiological Society of North America. Global radiologist shortage, May 2022. URL <https://www.rsna.org/news/2022/may/global-radiologist-shortage>.
- Mike Richards, Giles Maskell, Kath Halliday, and Martin Allen. Diagnostics: a major priority for the nhs. *Future healthcare journal*, 9(2):133, 2022.
- M Winder, AJ Owczarek, J Chudek, J Pilch-Kowalczyk, and J Baron. Are we overdoing it? changes in diagnostic imaging workload during the years 2010-2020 including the impact of the sars-cov-2 pandemic. *healthcare (basel)*, 2021.
- Daiju Ueda, Toshimasa Matsumoto, Shoichi Ehara, Akira Yamamoto, Shannon L Walston, Asahiro Ito, Taro Shimono, Masatsugu Shiba, Tohru Takeshita, Daiju Fukuda, et al. Artificial intelligence-based model to classify cardiac functions from chest radiographs: a multi-institutional, retrospective model development and validation study. *The Lancet Digital Health*, 5(8):e525–e533, 2023.
- Balaji Rao, Vahe Zohrabian, Paul Cedeno, Atin Saha, Jay Pahade, and Melissa A Davis. Utility of artificial intelligence tool as a prospective radiology peer reviewer—detection of unreported intracranial hemorrhage. *Academic radiology*, 28(1):85–93, 2021.
- Erdi Çağlı, Ecem Sogancioglu, Bram van Ginneken, Kicky G van Leeuwen, and Keelin Murphy. Deep learning for chest x-ray analysis: A survey. *Medical Image Analysis*, 72:102125, 2021.
- Boris Shirokikh, Alexandra Dalechina, Alexey Shevtsov, Egor Krivov, Valery Kostjuchenko, Amayak Durgaryan, Mikhail Galkin, Andrey Golanov, and Mikhail Belyaev. Systematic clinical evaluation of a deep learning method for medical image segmentation: radiosurgery application. *IEEE Journal of Biomedical and Health Informatics*, 26(7):3037–3046, 2022.
- Xiaoxuan Liu, Livia Faes, Aditya U Kale, Siegfried K Wagner, Dun Jack Fu, Alice Bruynseels, Thushika Mahendiran, Gabriella Moraes, Mohith Shamdas, Christoph Kern, et al. A comparison of deep learning performance against health-care professionals in detecting diseases from medical imaging: a systematic review and meta-analysis. *The lancet digital health*, 1(6):e271–e297, 2019.
- Larisa Gorenstein, Shelly Soffer, Sara Apter, Eli Konen, and Eyal Klang. Ai in radiology: is it the time for randomized controlled trials? *European Radiology*, 33(6):4223–4225, 2023.
- Souhail Bennani, Nor-Eddine Regnard, Jeanne Ventre, Louis Lassalle, Toan Nguyen, Alexis Ducarouge, Lucas Dargent, Enora Guillo, Elodie Gouhier, Sophie-Hélène Zaimi, et al. Using ai to improve radiologist performance in detection of abnormalities on chest radiographs. *Radiology*, 309(3):e230860, 2023.

- Jong Seok Ahn, Shadi Ebrahimian, Shaunagh McDermott, Sanghyup Lee, Laura Naccarato, John F Di Capua, Markus Y Wu, Eric W Zhang, Victorine Muse, Benjamin Miller, et al. Association of artificial intelligence–aided chest radiograph interpretation with reader performance and efficiency. *JAMA Network Open*, 5(8):e2229289–e2229289, 2022.
- David K Eng, Nishith B Khandwala, Jin Long, Nancy R Fefferman, Shailee V Lala, Naomi A Strubel, Sarah S Milla, Ross W Filice, Susan E Sharp, Alexander J Towbin, et al. Artificial intelligence algorithm improves radiologist performance in skeletal age assessment: a prospective multicenter randomized controlled trial. *Radiology*, 301(3): 692–699, 2021.
- Basel Yacoub, Akos Varga-Szemes, U Joseph Schoepf, Ismail M Kabakus, Dhiraj Baruah, Jeremy R Burt, Gilberto J Aquino, Allison K Sullivan, Jim O’ Doherty, Philipp Hoelzer, et al. Impact of artificial intelligence assistance on chest ct interpretation times: a prospective randomized study. *American Journal of Roentgenology*, 219(5):743–751, 2022.
- Andres F Abadia, Basel Yacoub, Natalie Stringer, Madalyn Snoddy, Madison Kocher, U Joseph Schoepf, Gilberto J Aquino, Ismail Kabakus, Danielle Dargis, Philipp Hoelzer, et al. Diagnostic accuracy and performance of artificial intelligence in detecting lung nodules in patients with complex lung disease: a noninferiority study. *Journal of Thoracic Imaging*, 37(3):154–161, 2022.
- Heber MacMahon, David P Naidich, Jin Mo Goo, Kyung Soo Lee, Ann NC Leung, John R Mayo, Atul C Mehta, Yoshiharu Ohno, Charles A Powell, Mathias Prokop, et al. Guidelines for management of incidental pulmonary nodules detected on ct images: from the fleischner society 2017. *Radiology*, 284(1):228–243, 2017.
- Marco Francone, Franco Iafrate, Giorgio Maria Masci, Simona Coco, Francesco Cilia, Lucia Manganaro, Valeria Panebianco, Chiara Andreoli, Maria Chiara Colaiacomo, Maria Antonella Zingaropoli, et al. Chest ct score in covid-19 patients: correlation with disease severity and short-term prognosis. *European radiology*, 30:6808–6817, 2020.
- Mariaelena Occhipinti, Matteo Paoletti, Brian J Bartholmai, Srinivasan Rajagopalan, Ronald A Karwoski, Cosimo Nardi, Riccardo Inchingolo, Anna R Larici, Gianna Camiciottoli, Federico Lavorini, et al. Spirometric assessment of emphysema presence and severity as measured by quantitative ct and ct-based radiomics in copd. *Respiratory Research*, 20:1–11, 2019.
- Vinaya S Karkhanis and Jyotsna M Joshi. Pleural effusion: diagnosis, treatment, and management. *Open access emergency medicine: OAEM*, 4:31, 2012.
- Reginald F Munden, Brett W Carter, Caroline Chiles, Heber MacMahon, William C Black, Jane P Ko, H Page McAdams, Santiago E Rossi, Ann N Leung, Phillip M Boiselle, et al. Managing incidental findings on thoracic ct: mediastinal and cardiovascular findings. a white paper of the acr incidental findings committee. *Journal of the American College of Radiology*, 15(8):1087–1096, 2018.
- European Society of Cardiology. Aortic diseases clinical practice guidelines. URL <https://www.escardio.org/Guidelines/Clinical-Practice-Guidelines/Aortic-Diseases>.
- Daniel I Glazer and William W Mayo-Smith. Management of incidental adrenal masses: an update. *Abdominal Radiology*, 45:892–900, 2020.
- Zhe He, Dongsheng Zhang, Haiping Xiao, Qihang Zhu, Yiwen Xuan, Kai Su, Ming Liao, Yong Tang, and Enwu Xu. The ideal methods for the management of rib fractures. *Journal of thoracic Disease*, 11(Suppl 8):S1078, 2019.
- Harry K Genant, Chun Y Wu, Cornelis Van Kuijk, and Michael C Nevitt. Vertebral fracture assessment using a semiquantitative technique. *Journal of bone and mineral research*, 8(9):1137–1148, 1993.
- International Society for Clinical Densitometry. Official positions 2023, 2023. URL <https://iscd.org/official-positions-2023/>.
- Sian Taylor-Phillips and Chris Stinton. Fatigue in radiology: a fertile area for future research. *The British journal of radiology*, 92(1099):20190043, 2019.
- Maria De La Iglesia Vayá, Jose Manuel Saborit, Joaquim Angel Montell, Antonio Pertusa, Aurelia Bustos, Miguel Cazorla, Joaquin Galant, Xavier Barber, Domingo Orozco-Beltrán, Francisco García-García, et al. Bimcv covid-19+: a large annotated dataset of rx and ct images from covid-19 patients. *arXiv preprint arXiv:2006.01174*, 2020.
- ME Gatt, G Spectre, O Paltiel, N Hiller, and R Stalnikowicz. Chest radiographs in the emergency department: is the radiologist really necessary? *Postgraduate medical journal*, 79(930):214–217, 2003.

5 Supplementary

5.1 Experiment report template

Participants in each arm filled up a structured report in an editable web form during CT reading. In the case of Control and Informed arms, the report for each CT study was pre-filled with the standard “no pathologies present” template, see Table 6. In the experimental arm, while working with DLA, it was prefilled with DLA findings, see example in Table 6.

Table 4: Total number of findings by pathology in different groups.

Group/pathology	Lymph nodes	Coronary calcium	Pulmonary trunk	COVID	Ribs	Pleural effusion	Adrenal	Genant	Lung nodules	Emphysema	Osteoporosis	Aorta	Total
Ground Truth	45	120	66	73	29	51	40	27	27	67	109	42	696
Control (no AI)	27	73	17	100	8	45	6	9	40	48	0	9	382
With AI-aid training	41	71	45	113	12	47	19	18	39	58	14	31	508
Experimental without AI	36	91	43	111	22	48	24	23	38	59	54	24	573
Experimental with AI	53	116	72	103	54	53	40	38	46	65	118	52	810
BIMCV annotation	24	24	12	93	3	43	7	4	27	23	1	8	269
AI	57	103	67	100	61	65	44	37	48	66	118	53	819

Table 5: Number of ground truth findings stratified by different severity levels.

Severity	Lymph nodes	Coronary calcium	Pulmonary trunk	COVID	Ribs	Pleural effusion	Adrenal	Genant	Lung nodules	Emphysema	Osteoporosis	Aorta	Total
Low	4	42	14	52	29	31	0	0	5	52	51	0	280
Moderate	30	28	29	14	0	20	12	21	6	9	58	42	269
Severe	11	50	23	7	0	0	28	6	16	6	0	0	147
Total	45	120	66	73	29	51	40	27	27	67	109	42	696

5.2 Text annotation

Annotation of BIMCV original medical reports, and readings prepared by experiment participants was performed manually by two experts, in case of disagreement consensus decision was made by a third expert (agreement rate was over 97%). During text annotation experts were asked to mark whether any condition related to a specific pathology was present (pathology marked as “positive”), or it was clearly stated that there is no description of pathology (marked as “negative”). If pathology or any condition related to this pathology was not mentioned in the report, then the pathology was marked as “not mentioned”. After annotation, the “not mentioned” class was converted to “negative”.

5.3 DLA system details

The DLA system is based on two components. First, a set of deep convolutional neural networks based on a Feature Pyramid Network architecture, which are used to automate morphological measurements and/or segment regions of interest on the volumetric CT image. Second, a rule based text-system which generates a text report from the morphological measurements based on international guidelines, see Table 1 for the guidelines, see Table 6 for example of the generated report.

Results of the first component are displayed on a DICOM study in the form of burned-in coloured overlay. Interface highlight schema varies depending on pathology (diameters, contours, or boxes), see Figures 4, 5, 6. A generated text report is provided in the DICOM Structured Report format.

5.4 BIMCV dataset statistic

We have used 200 studies from the first release of BIMCV-COVID19 dataset, see Figure 7 for data selection profile. Table 4 provides information on pathologies frequency (ground truth, and in different experiment arms). Table 3 provides information of ground truth findings stratified by different severity levels.

5.5 Participants-wise and pathologies-wise metrics.

Tables 8 and 7 provide classification metrics for individual radiologists (averaged over 12 pathologies) and for individual pathologies, averaged over radiologists.

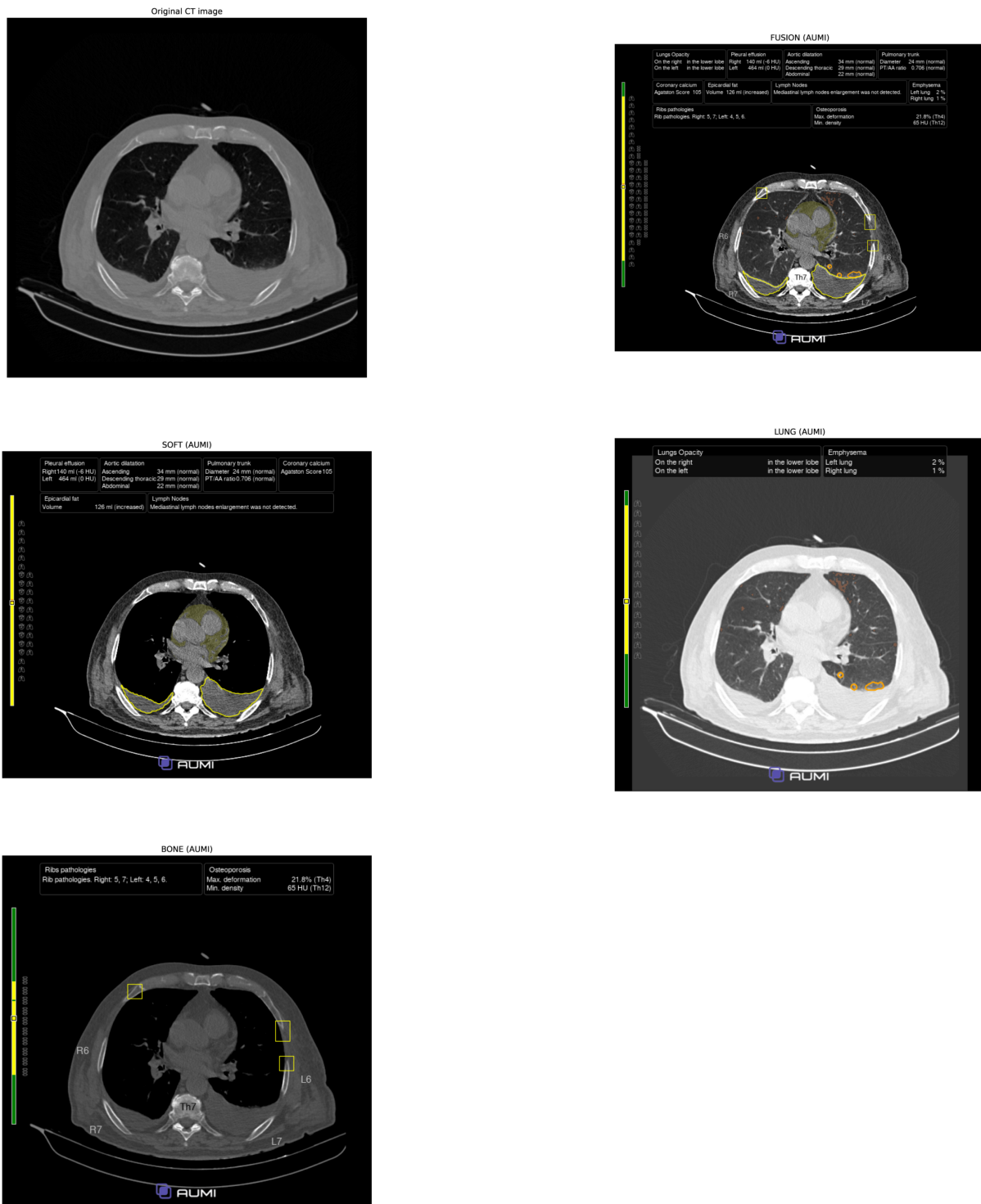


Figure 4: Original CT image and four CT windows provided by DLA: Fusion, Abdomen (SOFT), Lung, Bone. Best viewed in color.

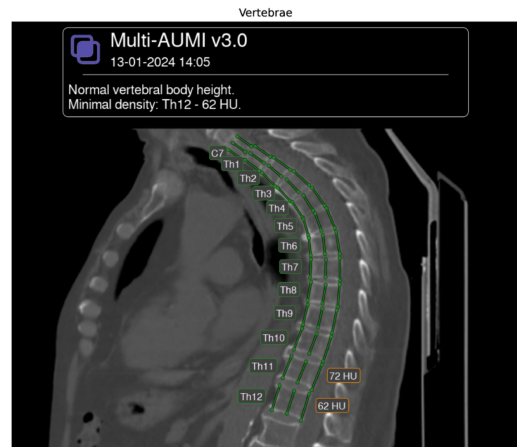
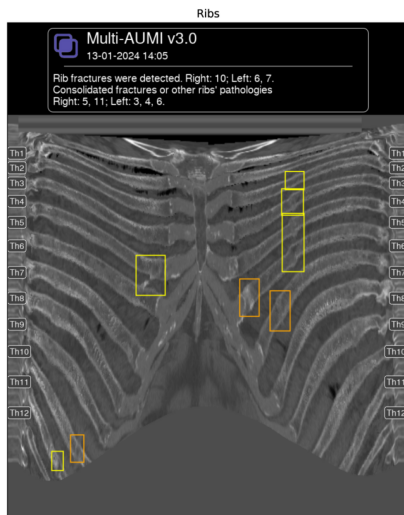
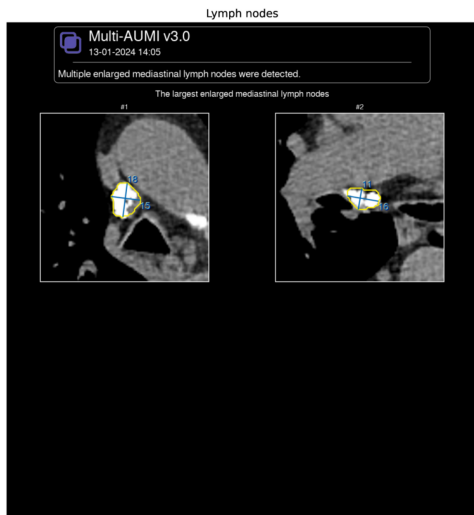
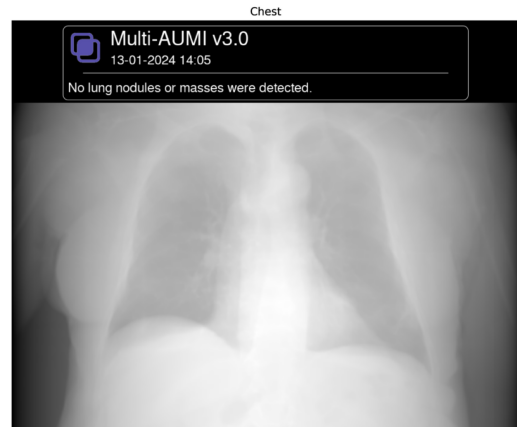
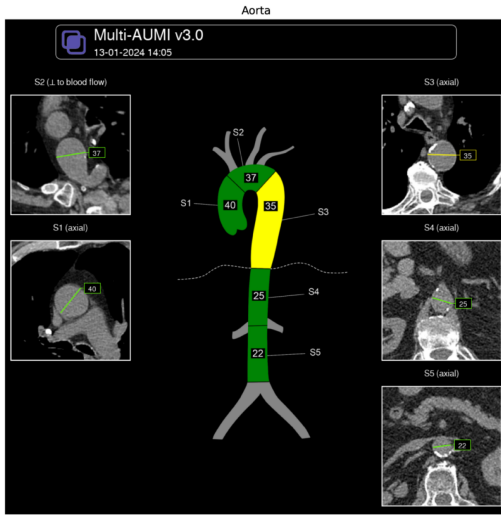


Figure 5: Summary images provided as first images in processed CT series for each finding: aorta, lungs, mediastinal lymph node, pulmonary trunk, ribs fractures, vertebrae with Genant index measurements. Best viewed in color.

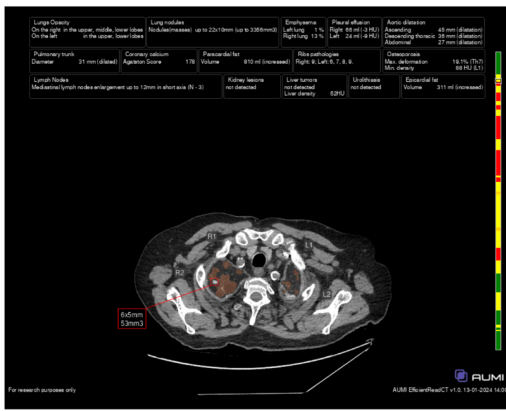
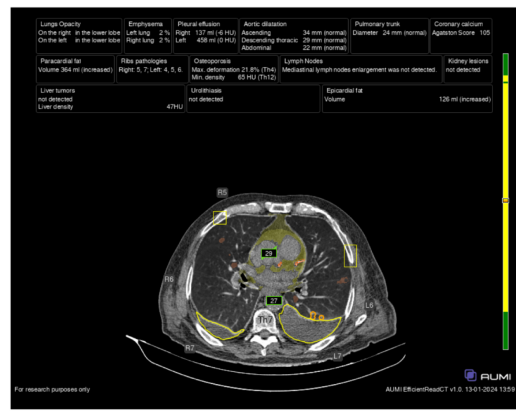
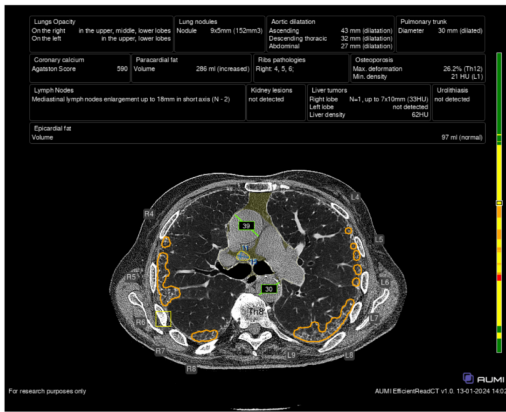
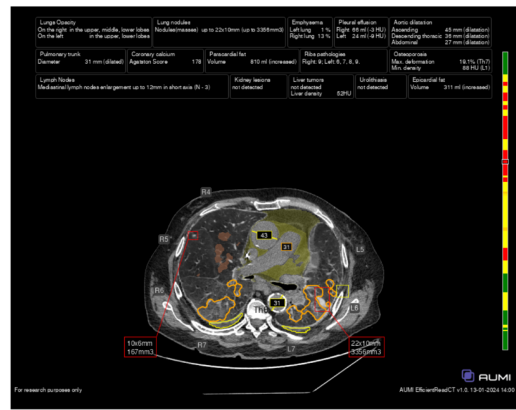
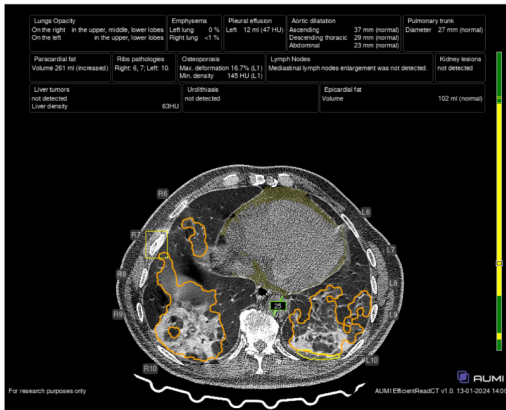


Figure 6: Example findings. Different DLA findings are overlaid over 2D axial slices of the processed DICOM series. COVID-19 features, consolidated ribs fracture; pulmonary trunk enlargement, aorta enlargement, pleural effusion, lung nodules, features of emphysema, and COVID-19; enlarged lymph nodes, features of COVID-19; pleural effusion, features of emphysema, calcifications; lung nodules, features of emphysema. Best viewed in color.

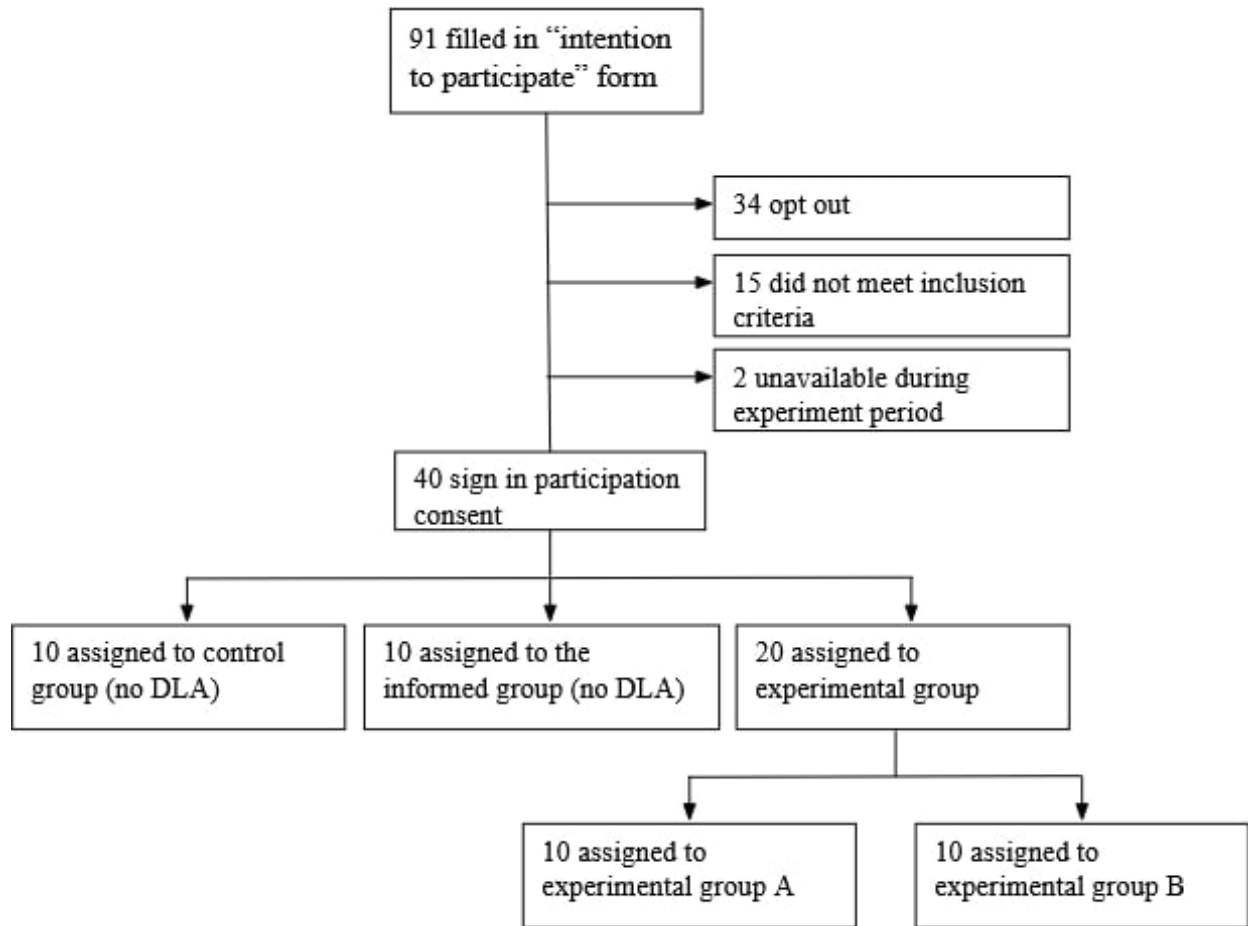


Figure 7: Participated radiologists profile.

Table 7: Pathology-wise metrics in all groups.

Group	Pathology	Precision	Sensitivity	Specificity	F1	Accuracy
Control (no AI)	adrenal	83.3	12.5	99.4	21.7	82.0
Control (no AI)	aorta	33.3	7.1	96.2	11.8	77.5
Control (no AI)	coronary calcium	95.9	58.3	96.2	72.5	73.5
Control (no AI)	covid	69.0	94.5	75.6	79.8	82.5
Control (no AI)	emphysema	93.8	67.2	97.7	78.3	87.5
Control (no AI)	genant	88.9	29.6	99.4	44.4	90.0
Control (no AI)	lung nodules	37.5	55.6	85.5	44.8	81.5
Control (no AI)	lymph nodes	88.9	53.3	98.1	66.7	88.0
Control (no AI)	pleural effusion	88.9	78.4	96.6	83.3	92.0
Control (no AI)	pulmonary trunk	94.1	24.2	99.3	38.6	74.5
Control (no AI)	ribs	62.5	17.2	98.2	27.0	86.5
Control (no AI)	osteoporosis	-	0.0	100.0	-	45.5
With AI-aid training	adrenal	57.9	27.5	95.0	37.3	81.5
With AI-aid training	aorta	54.8	40.5	91.1	46.6	80.5
With AI-aid training	coronary calcium	93.0	55.0	93.8	69.1	70.5
With AI-aid training	covid	59.3	91.8	63.8	72.0	74.0
With AI-aid training	emphysema	86.2	74.6	94.0	80.0	87.5
With AI-aid training	genant	77.8	51.9	97.7	62.2	91.5
With AI-aid training	lung nodules	51.3	74.1	89.0	60.6	87.0
With AI-aid training	lymph nodes	58.5	53.3	89.0	55.8	81.0

With AI-aid training	pleural effusion	80.9	74.5	94.0	77.6	89.0
With AI-aid training	pulmonary trunk	75.6	51.5	91.8	61.3	78.5
With AI-aid training	ribs	83.3	34.5	98.8	48.8	89.5
With AI-aid training	osteoporosis	100.0	12.8	100.0	22.8	52.5
Experimental without AI	adrenal	79.2	47.5	96.9	59.4	87.0
Experimental without AI	aorta	66.7	38.1	94.9	48.5	83.0
Experimental without AI	coronary calcium	94.5	71.7	93.8	81.5	80.5
Experimental without AI	covid	63.1	95.9	67.7	76.1	78.0
Experimental without AI	emphysema	79.7	70.1	91.0	74.6	84.0
Experimental without AI	genant	78.3	66.7	97.1	72.0	93.0
Experimental without AI	lung nodules	47.4	66.7	88.4	55.4	85.5
Experimental without AI	lymph nodes	69.4	55.6	92.9	61.7	84.5
Experimental without AI	pleural effusion	89.6	84.3	96.6	86.9	93.5
Experimental without AI	pulmonary trunk	81.4	53.0	94.0	64.2	80.5
Experimental without AI	ribs	81.8	62.1	97.7	70.6	92.5
Experimental without AI	osteoporosis	94.4	46.8	96.7	62.6	69.5
Experimental with AI	adrenal	80.0	80.0	95.0	80.0	92.0
Experimental with AI	aorta	80.8	100.0	93.7	89.4	95.0
Experimental with AI	coronary calcium	96.6	93.3	95.0	94.9	94.0
Experimental with AI	covid	68.9	97.3	74.8	80.7	83.0
Experimental with AI	emphysema	86.2	83.6	93.2	84.8	90.0
Experimental with AI	genant	71.1	100.0	93.6	83.0	94.5
Experimental with AI	lung nodules	52.2	88.9	87.3	65.8	87.5
Experimental with AI	lymph nodes	67.9	80.0	89.0	73.5	87.0
Experimental with AI	pleural effusion	88.7	92.2	96.0	90.4	95.0
Experimental with AI	pulmonary trunk	83.3	90.9	91.0	87.0	91.0
Experimental with AI	ribs	51.9	96.6	84.8	67.5	86.5
Experimental with AI	osteoporosis	89.0	96.3	85.7	92.5	91.5
Automated (no radiologist)	adrenal	79.5	87.5	94.4	83.0	93.0
Automated (no radiologist)	aorta	79.2	100.0	93.0	88.4	94.5
Automated (no radiologist)	coronary calcium	98.1	84.2	97.5	90.6	89.5
Automated (no radiologist)	covid	67.0	91.8	74.0	77.5	80.5
Automated (no radiologist)	emphysema	83.3	82.1	91.7	82.7	88.5
Automated (no radiologist)	genant	73.0	100.0	94.2	84.4	95.0
Automated (no radiologist)	lung nodules	54.2	96.3	87.3	69.3	88.5
Automated (no radiologist)	lymph nodes	59.6	75.6	85.2	66.7	83.0
Automated (no radiologist)	pleural effusion	76.9	98.0	89.9	86.2	92.0
Automated (no radiologist)	pulmonary trunk	85.1	86.4	92.5	85.7	90.5
Automated (no radiologist)	ribs	45.9	96.6	80.7	62.2	83.0
Automated (no radiologist)	osteoporosis	74.6	80.7	67.0	77.5	74.5
BIMCV annotation	adrenal	57.1	10.0	98.1	17.0	80.5
BIMCV annotation	aorta	37.5	7.1	96.8	12.0	78.0
BIMCV annotation	coronary calcium	100.0	20.0	100.0	33.3	52.0
BIMCV annotation	covid	73.1	93.2	80.3	81.9	85.0
BIMCV annotation	emphysema	95.7	32.8	99.2	48.9	77.0
BIMCV annotation	genant	75.0	11.1	99.4	19.4	87.5
BIMCV annotation	lung nodules	66.7	66.7	94.8	66.7	91.0
BIMCV annotation	lymph nodes	62.5	33.3	94.2	43.5	80.5
BIMCV annotation	pleural effusion	90.7	76.5	97.3	83.0	92.0
BIMCV annotation	pulmonary trunk	75.0	13.6	97.8	23.1	70.0
BIMCV annotation	ribs	100.0	10.3	100.0	18.8	87.0
BIMCV annotation	osteoporosis	100.0	0.9	100.0	1.8	46.0

Table 8: Radiologists-wise metrics averaged over 12 pathologies.

Group	Radiologist	Precision	Sensitivity	Specificity	F1	Accuracy
-------	-------------	-----------	-------------	-------------	----	----------

Workload of radiologist

Control (no AI)	1	34.3	60.5	78.2	43.8	75.4
Control (no AI)	2	57.7	76.9	89.1	65.9	87.1
Control (no AI)	5	30.1	78.6	75.9	43.6	76.2
Control (no AI)	7	60.5	87.5	82.6	71.5	83.8
Control (no AI)	8	33.8	73.3	79.5	46.3	78.8
Control (no AI)	13	52.1	78.7	82.4	62.7	81.7
Control (no AI)	17	31.6	86.2	74.4	46.3	75.8
Control (no AI)	25	43.6	73.9	77.3	54.8	76.7
Control (no AI)	28	51.0	83.3	88.6	63.3	87.9
Control (no AI)	36	40.7	84.6	76.1	55.0	77.5
With AI-aid training	0	62.8	74.2	83.3	68.1	80.8
With AI-aid training	4	46.2	81.1	82.8	58.8	82.5
With AI-aid training	9	44.2	69.7	86.0	54.1	83.8
With AI-aid training	11	61.2	83.3	90.7	70.6	89.6
With AI-aid training	18	65.8	73.2	84.0	69.3	80.8
With AI-aid training	21	55.6	61.6	78.4	58.4	73.3
With AI-aid training	22	53.5	84.4	83.1	65.5	83.3
With AI-aid training	35	49.4	81.6	78.5	61.5	79.2
With AI-aid training	37	61.6	75.0	84.4	67.7	82.1
With AI-aid training	39	19.4	34.2	73.3	24.8	67.1
Experimental without AI	3	81.6	88.6	91.8	84.9	90.8
Experimental without AI	6	65.9	84.4	84.1	74.0	84.2
Experimental without AI	10	69.2	85.7	91.9	76.6	90.8
Experimental without AI	12	62.5	75.0	91.0	68.2	88.3
Experimental without AI	14	85.2	62.2	95.2	71.9	85.0
Experimental without AI	15	77.5	86.1	89.3	81.6	88.3
Experimental without AI	16	78.0	86.5	89.2	82.1	88.3
Experimental without AI	19	60.0	85.7	82.6	70.6	83.3
Experimental without AI	20	81.8	81.8	95.9	81.8	93.3
Experimental without AI	23	41.0	69.6	76.3	51.6	75.0
Experimental without AI	24	40.5	78.9	78.2	53.6	78.3
Experimental without AI	26	71.8	82.4	87.2	76.7	85.8
Experimental without AI	27	57.1	76.2	87.9	65.3	85.8
Experimental without AI	29	61.4	75.0	79.8	67.5	78.3
Experimental without AI	30	77.8	81.4	87.0	79.5	85.0
Experimental without AI	31	85.2	71.9	95.5	78.0	89.2
Experimental without AI	32	53.3	69.6	85.6	60.4	82.5
Experimental without AI	33	46.4	61.9	84.8	53.1	80.8
Experimental without AI	34	51.2	78.6	77.2	62.0	77.5
Experimental without AI	38	43.2	64.0	77.9	51.6	75.0
Experimental with AI	3	95.3	78.8	97.1	86.3	89.2
Experimental with AI	6	85.0	91.9	92.8	88.3	92.5
Experimental with AI	10	97.4	86.4	98.7	91.6	94.2
Experimental with AI	12	96.4	73.0	98.8	83.1	90.8
Experimental with AI	14	97.7	81.1	98.5	88.7	90.8
Experimental with AI	15	94.9	86.0	97.4	90.2	93.3
Experimental with AI	16	100.0	82.2	100.0	90.2	93.3
Experimental with AI	19	97.6	88.9	98.7	93.0	95.0
Experimental with AI	20	96.3	74.3	98.8	83.9	91.7
Experimental with AI	23	90.0	76.6	94.5	82.8	87.5
Experimental with AI	24	87.8	76.6	93.2	81.8	86.7
Experimental with AI	26	88.5	69.7	96.6	78.0	89.2
Experimental with AI	27	83.3	71.4	95.7	76.9	90.0
Experimental with AI	29	85.2	74.2	95.5	79.3	90.0
Experimental with AI	30	100.0	77.8	100.0	87.5	93.3
Experimental with AI	31	100.0	55.0	100.0	71.0	85.0
Experimental with AI	32	89.2	78.6	94.9	83.5	89.2
Experimental with AI	33	82.2	86.0	89.6	84.1	88.3
Experimental with AI	34	86.8	89.2	94.0	88.0	92.5

Workload of radiologist

Experimental with AI	38	86.7	74.3	95.3	80.0	89.2
----------------------	----	------	------	------	------	------

Table 6: Example of the form used in the experiment. Anamnesis was extracted from existing clinical history in both cases.

Field		"No pathologies present" template	Example report filled from DLA findings
Medical history (anamnesis)	history	73 y.o. man. Complaints of cough and shortness of breath.	77 y.o. man. Oncology screening.
Lungs		No focal or infiltrative changes. The trachea and large bronchi are unchanged. No pleural effusion detected.	A nodule measuring 15x12mm (average size 14mm according to Fleischner), with a volume of 915mm ³ , is identified in the right lung. Changes in the lungs with a low probability of COVID-19 are determined. Areas of emphysematous changes less than 6% are identified in the lungs. The percentage of right lung involvement is 2%, left lung 1%, both lungs 2%. The trachea and large bronchi are unchanged. A 17 ml effusion with an average density of 32 HU is identified in the right pleural cavity. No effusion is identified in the left pleural cavity.
Mediastinum		Unchanged, no effusion in the pericardial cavity.	Unchanged, no effusion in the pericardial cavity.
Cardiovascular System	Sys-	The aorta and pulmonary trunk are unchanged.	The descending section of the thoracic aorta is expanded to 33 mm (dilation). Other sections of the aorta at the examined level are not expanded. The pulmonary trunk is not expanded (up to 26 mm). Pulmonary-aortic index - 0.722. Coronary artery calcification is determined - Agatston Index: 42, CAC-DRS 1.
Lymph Nodes		Not enlarged.	Not enlarged.
Soft Tissues		Unchanged.	Unchanged.
Skeletal System		No focal, destructive, or traumatic changes.	Consolidated rib fractures: Right: 4 in the anterior third. Left: 2 in the anterior third. Compression deformation of the Th12 vertebrae body is detected - 30.5%. A decrease in the mineral density of the vertebral bodies' bone tissue is detected: Th11 - 41 HU, Th12 - 42 HU.
Abdominal Organs		No changes detected in the scanned area.	No changes detected in the scanned area.
Conclusion		No focal or infiltrative changes detected in the lungs.	Changes in the lungs, low probability of COVID-19, have been identified. A nodule in the right lung has been identified. CT in dynamics is recommended in 6 months. Areas of emphysematous changes less than 6% are identified in the lungs. Right-sided pleural effusion. Dilation of the descending thoracic section of the aorta has been identified. Other sections of the aorta at the examined level are not expanded. Cardiologist consultation is recommended. Agatston Index: 42 (CAC-DRS 1) - minor calcification. Consolidated rib fractures: Right: 4; Left: 2. Compression deformation of the Th12 vertebrae body (Genant 2) has been identified. A decrease in the mineral density of the bone tissue, corresponding to osteoporosis, has been identified. Endocrinologist consultation is recommended.